Hover Handling Qualities of Fixed-Pitch, Variable-RPM Quadcopters with Increasing Rotor Diameter

Ariel Walter PhD Student
Michael McKay PhD Student
Robert Niemiec Research Scientist
Farhan Gandhi Redfern Professor, Director

Center for Mobility with Vertical Lift (MOVE)
Rensselaer Polytechnic Institute
Troy, NY United States

Christina Ivler
Assistant Professor
University of Portland
Portland, OR United States

ABSTRACT

The handling qualities of quadcopters with fixed-pitch, variable-RPM rotors of several diameters are examined. Three aircraft sizes are considered, with rotor diameters of 1.2, 1.8, and 2.4 meters and gross weights of 136, 308, and 544 kg respectively. Each aircraft is first held to standard, ADS-33 handling qualities specifications, then Froude-scaled specifications are applied in order to scale the requirements of the two smaller aircraft. CONDUIT® is used to optimize inner and outer loop controllers for actuator activity in each case. Time domain simulations are then presented in order to determine the necessary motor current margins needed. In the time domain, piloted commands and gust inputs are simulated along all axes for both the inner and outer loop controllers. Much greater current is required for yaw rate commands than for either pitch or roll commands. However, when a TRC controller is included, significantly higher current margin is needed during a small magnitude step in longitudinal speed for all aircraft sizes than were observed for the inner loop. The maneuver that requires the highest current margin is the yaw rate step for the smallest aircraft and the longitudinal velocity step for the others, regardless of Foude-scaling. Using the maximum current values from these simulations, the 136 kg vehicle requires 9.7% to 12.4% motor weight fraction, the 308kg vehicle 13.0% to 14.4% motor weight fraction, and the 544 kg vehicle requires a motor weight fraction of 16.8%. Motor weight requirements can be reduced somewhat on the larger aircraft by flying the pitch and roll axes exclusively in ACAH mode instead of TRC mode. In this case, step commands in yaw rate is limiting for the 308 kg vehicle (requiring 12.0%–13.1% motor weight fraction) and heave commands are limiting for the 544kg vehicle (requiring 14.5% motor weight fraction).

NOTATION

Symbols

i	Motor Current
I_{rotor}	Rotor Inertia
K	OLOP Constant
K_e	Motor back-EMF Constant
K_t	Motor Torque Constant
L	Motor Inductance
N_{rotors}	Number of Rotors
r	Yaw Rate
R	Rotor Radius
R_m	Motor Resistance
Q	Motor Torque
Q_A	Rotor Aerodynamic Torque
u	Longitudinal Velocity
U	Control Inputs
v	Lateral Velocity
V	Motor Voltage
w	Heave Rate
X	Dynamic States
Ω	Rotor Speed
$\dot{\Omega}$	Rotor Acceleration
ϕ	Roll Attitude
θ	Pitch Attitude
ψ	Heading
Ψ	Azimuthal Location

Acronyms

ACAH	Attitude Command, Attitude Hold
eVTOL	Electric Vertical Takeoff and Landing
FB	Feed-Back
FF	Feed-Forward
HQ	Handling Qualities
OLOP	Open-Loop-Onset-Point
RCDH	Rate Command, Direction Hold
RMAC	Rensselaer Multicopter Analysis Code

Presented at the VFS International 76th Annual Forum & Technology Display, Virginia Beach, Virginia, October 6–8, 2020.

RMS Root Mean Square
TRC Translational Rate Command

INTRODUCTION

With the push for the development of Urban Air Mobility (UAM), a large variety of electric Vertical Takeoff and Landing (eVTOL) aircraft configurations and designs have been proposed, but the field still faces many challenges before large eVTOL aircraft become commonplace (Ref. 1). One of these challenges is the scalability of fixed-pitch, variable-RPM multirotor systems, which are common on eVTOL aircraft.

One barrier to scaling up fixed-pitch rotors on electric aircraft is their ability to meet handling qualities (flying qualities) requirements. Though fixed-pitch, variable-RPM rotors have been used for small-scale, unmanned multirotor aircraft for years, their effectiveness on larger, manned-sized vehicles is still under examination. Handling qualities (HQ) requirements specific to these aircraft have not yet been officially established, but the current Aeronautical Design Standard, ADS-33E-PRF (Ref. 2), defines HQ metrics for manned military helicopters. Another important requirement defined for manned aircraft is disturbance rejection (Ref. 3). It has previously been shown (Ref. 4) that large eVTOL aircraft which rely on changing the rotational speed of large rotors for control may not be able to meet disturbance rejection bandwidth requirements without a significantly higher installed power (and thus, weight) than would otherwise be required on such an aircraft.

The purpose of this study is to examine the effects of increasing rotor size on the motors required for a variable-RPM quadcopter to meet HQ specifications from the ADS-33E-PRF and disturbance rejection requirements from Ref. 3. A manned size (1200 lb) quadcopter will be considered as a baseline, as well as smaller aircraft at equivalent disk loading. The metrics defined in the ADS-33E-PRF have previously been applied to smaller, non-manned aircraft, such as Ref. 5 where Froude-scaling is applied to obtain scaled requirements for the IRIS+ Quadcopter by a scaling to the maximum velocity of the UH-60 Black Hawk.

Similarly, length-based Froude-scaling was used in Ref. 4 to examine the scaling of HQ specifications on quadcopters of different sizes. This previous study found that, with a motor power saturation limit included, larger fixed-pitch, variable-RPM quadcopters were unable to meet disturbance rejection bandwidth requirements with typical installed power, especially in yaw. the present study instead relaxes the installed power (motor size) constraint and examines similar quadrotor aircraft in order to determine the motor size actually required for the aircraft to perform adequately with respect to published HQ requirements.

MODELING AND ANALYSIS TOOLS

Platform

The aircraft considered in this study are cross-type quadcopters with a tip clearance of 10% of the rotor radius. Each rotor is directly-driven by a dedicated electric motor. A simple representation of the quadcopter configuration, including rotor/motor numbering and spin direction, is shown in Fig. 1. Scaled aircraft with 1.2, 1.8, and 2.4 m (4, 6, and 8 ft) rotor diameters are simulated, with the use of 1.2 m diameter rotors considered to be at the lower end of the range of interest for UAM applications. The disk loading is held constant at 287 N/m^2 (6 lb/ft^2) for all vehicle sizes considered, resulting in aircraft gross weights of 136, 308, and 544 kg (300, 680, and 1200 lb).

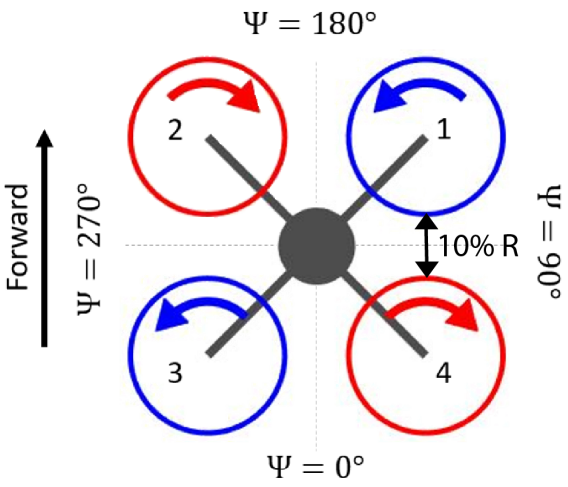

Figure 1: Quadcopter Configuration with Rotor Numbering

The rotor geometry used on these quadcopters is summarized in Table 1. The rotors are scaled based on their diameter for use on the large quadcopters simulated here, holding non-dimensional quantities, such as the solidity and taper ratio, constant.

Table 1: Rotor Geometry

Parameter	Value
Rotor Solidity	0.09
Taper Ratio	2.5
Root Pitch	21.5°
Tip Pitch	11.1°

The rotational inertia of the fuselage is based on a scaled version of the NASA Concept quadcopter presented in Ref. 1. These scaled inertias, as well as the hover current and power input to each motor, are given in Table 2.

Simulation Models

Dynamic simulation models are generated using the Rensselaer Multicopter Analysis Code (RMAC) (Ref. 6). This code calculates the forces and moments on the multicopter using blade element theory coupled with a 3x4 Peter-He finite state dynamic wake model. The dynamic states include the 12 rigid-body states (position, attitude, linear velocity, and angular rate), 10 inflow states per rotor (40 total), and the four rotor

Table 2: Aircraft Parameters

Rotor Diameter (m)	1.2	1.8	2.4
Gross Weight (kg)	136	308	544
Rotor Weight (kg)	0.67	2.27	5.38
Rotor Inertia (kg m^2)	0.063	0.480	2.014
Hover Current (A)	75	112	150
Hover Torque (N m)	22.5	73.9	177
Total Hover Power (kW)	21	48	85
I_{xx} (kg m^2)	43	173	467
I_{yy} (kg m^2)	51	204	549
I_{zz} (kg m^2)	84	334	905
K_e and K_t	0.30	0.66	1.18

speeds. The inputs to the system are a voltage signal to each of the four motors. The inflow states are generally very high frequency (on the order of the rotor speed, Ref. 7), and can be removed from the state space representation of the system via static condensation, yielding a lower-order model with the state and control vectors given by Eqs. 1 and 2, respectively.

$$X = [x\ y\ z\ \phi\ \theta\ \psi\ u\ v\ w\ p\ q\ r\ \Omega_1\ \Omega_2\ \Omega_3\ \Omega_4] \quad (1)$$

$$U = [V_1\ V_2\ V_3\ V_4] \quad (2)$$

The motor-rotor dynamics are modeled using DC motor equations, as in Ref. 8. The angular acceleration of the motor-rotor system is represented by Eq. 3, where $K_t i$ represents the input motor torque, Q_A is the aerodynamic torque, and viscous losses are neglected. The motor current is represented by Eq. 4, where L is the motor inductance, V is the input voltage, K_e is the back-EMF constant, and $R_m i$ is the Ohmic voltage drop across the motor.

$$I_{rotor}\dot{\Omega} = K_t i - Q_A \quad (3)$$

$$L\frac{di}{dt} = V - K_e\Omega - R_m i \quad (4)$$

Since L is negligible (Ref. 8), it is assumed that the electrical dynamics settle instantaneously. Equation 4 can then be solved for i and substituted into Eq. 3 to get Eq. 5, where $K_e = K_t$ for SI units. This equation is implemented as the governing equation relating rotor speed to the voltage input to the motor. The motor parameters K_t and R_a are obtained using the methods of Ref. 8.

$$I_{rotor}\dot{\Omega} = \frac{K_t}{R_m}V - \frac{K_t^2}{R_m}\Omega - Q_A \quad (5)$$

Control mixing is achieved by the multi-rotor coordinate transform (Eq. 6, Ref. 9), where Ψ_k represents the azimuthal location of rotor k on the aircraft (See Fig. 1). Using the multi-rotor coordinate transform decouples the dynamics of the quadcopter, reducing it to a system of single-input, single-output systems, one each for the longitudinal, lateral, directional, and vertical axes.

$$\begin{bmatrix} V_1 \\ V_2 \\ V_3 \\ V_4 \end{bmatrix} = \begin{bmatrix} 1 & \sin(\Psi_1) & \cos(\Psi_1) & 1 \\ 1 & \sin(\Psi_2) & \cos(\Psi_2) & -1 \\ 1 & \sin(\Psi_3) & \cos(\Psi_3) & 1 \\ 1 & \sin(\Psi_4) & \cos(\Psi_4) & -1 \end{bmatrix} \begin{bmatrix} V_0 \\ V_{1s} \\ V_{1c} \\ V_d \end{bmatrix} \quad (6)$$

Control Optimization

The ADS-33E-PRF (Ref. 2) provides a series of HQ specifications for manned helicopters, such as required piloted bandwidth and minimum damping ratios. Additionally, disturbance rejection requirements, outlined in Ref. 3, along with Open-Loop Onset Point (OLOP) specifications are included in the analysis (Ref. 10). To meet these requirements,

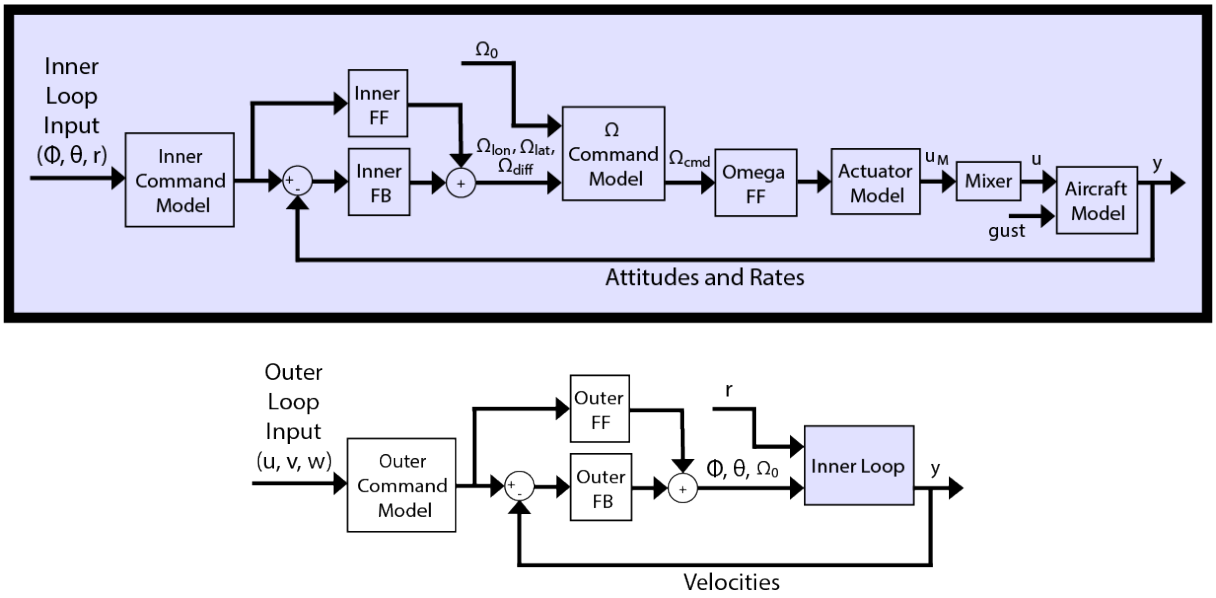

Figure 2: Controller Architecture

a 2DOF ACAH/RCDH explicit-model-following control architecture (Fig. 2) is implemented. The control optimization suite CONDUIT® (Ref. 11) optimizes the gains in the feedback controllers, as well as the command model frequencies, for actuator effort while meeting the specifications listed in Table 3.

After tuning the inner loop, the nested loop optimization approach of Ref. 11 is taken. The inner loop parameters are frozen, the inner loop specifications are disabled, and the outer loop specifications in Table 4 are used to optimize the gains of a translational-rate-command (TRC) controller.

An equivalent delay is included within each command model for both the inner and outer loop. This approximation of the delay accounts for the lag that is caused by the modeling of the motor dynamics and improves the model following at high frequency.

A critical specification in both the inner and outer loop is the Open Loop Onset Point (OLOP, Ref. 10) specification, which evaluates whether an aircraft is prone to undesired oscillations due to actuator rate saturation. For the multicopters considered in this study, the relevant rate limit is the acceleration of the rotors, which is directly proportional to the current that can be provided to the motors. If a motor is rated for K times the current required to hover, Eq. 3 yields

$$\dot{\Omega}_{\max} = \frac{K_t (K-1) i_{\text{hover}}}{I_{\text{rotor}}} \tag{7}$$

By reducing K until the OLOP specification is on the Level 1/2 boundary, a minimum required motor weight to avoid oscillations can be identified. The required current margin to meet the OLOP specification can then be found using Eq. 8.

$$\left(\frac{\Delta i}{i_{\text{hover}}}\right)_{\text{OLOP}} = (K-1) \tag{8}$$

In addition to the specifications suggested in Ref 11, the velocity rise time specification, RisLoG1, is added to the longitudinal and lateral HQ requirements for the TRC controller. This specification ensures that the TRC controller is sufficiently aggressive.

Scaling of Specifications

Two types of comparisons will be made between the three quadcopters considered in this study. In the first set of comparisons, all three multicopters will be held to the same standard, as defined by ADS-33. The second set of comparisons will utilize Froude-scaling (Ref. 12) to adjust the standards set by ADS-33, based on the presumption that a smaller vehicle is capable of greater agility. The Froude-scaling parameter is given by Eq. 9.

$$F = \sqrt{\frac{\text{Hub-to-Hub Distance}}{\text{Reference Hub-to-Hub Distance}}} \tag{9}$$

The reference hub-to-hub distance is that of the 1,200lb quadcopter. Thus, the largest of the quadcopters will be held to ADS-33 as is, while the standards will be scaled based on Table 5 for the two smaller vehicles.

Table 3: CONDUIT® Inner Loop Constraints

Specification	Axes
Hard Constraints	
EigLcG1	All
StbMgG1	Roll, Pitch, Yaw
NicMgG1	All
Soft Constraints	
BnwPiH1	Pitch
BnwRoH1	Roll
BnwYaH1	Yaw
CrsMnG2	Roll, Pitch, Yaw
DrbPiH1	Pitch
DrbRoH1	Roll
DrbYaH1	Yaw
DrpAvH1	Roll, Pitch, Yaw
EigDpG1	All
ModFoG1	Roll, Pitch, Yaw
OlpOpG1 (Pilot)	Roll, Pitch, Yaw
OlpOpG1 (Disturbance)	Roll, Pitch, Yaw
Summed Objectives	
RmsAcG1 (Pilot)	Roll, Pitch, Yaw
RmsAcG1 (Disturbance)	Roll, Pitch, Yaw
CrsLnG1	Roll, Pitch, Yaw

Table 4: CONDUIT® Outer Loop Constraints

Specification	Axes
Hard Constraints	
EigLcG1	All
StbMgG1	u, v, w
NicMgG1	u, v, w
Soft Constraints	
CrsMnG2	u, v, w
DrbVxH1	u
DrbVyH1	v
DrbVzH1	w
DrpAvH1	u, v, w
EigDpG1	All
FrqHeH1	w
ModFoG1	u, v, w
OlpOpG1 (Pilot)	u, v, w
OlpOpG1 (Disturbance)	u, v, w
RisLoG1	u,v
Summed Objectives	
RmsAcG1 (Pilot)	u, v, w
RmsAcG1 (Disturbance)	u, v, w
CrsLnG1	u, v, w

Table 5: Froude-Scaling of Different Dimensions

Dimension	Units	Scaling
Length	m	F^2
Time	s	F
Attitude	rad	-
Frequency	rad/s	$1/F$
Velocity	m/s	F

The roll bandwidth specification within CONDUIT® is shown as an example of how the specifications scale in Fig 3. Compared to the unscaled specification, the Froude-scaled version requires 41% higher bandwidth (rad/s) and 41% smaller phase delay (s) to reach Level 1.

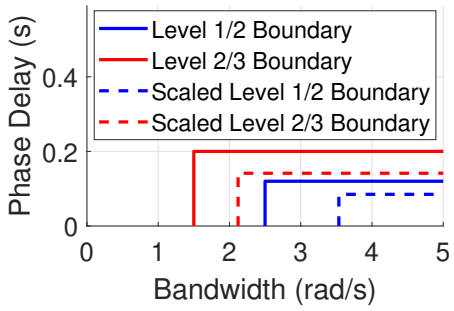

Figure 3: Roll Bandwidth Specification for Quadcopter with 1.2 m Diameter Rotors

RESULTS

Inner Loop Control Design

Optimized ACAH controllers are designed for each of the five aircraft cases that meet Level 1 HQ requirements for the specifications listed in Table 3. Full explanation of each of these specifications can be found in Ref. 11.

Tables 6 and 7 give the optimized values of the handling qualities specifications along the roll, pitch, and yaw axes (roll and pitch are combined since they are practically identical and use the same gains). The limiting specifications (those that are near the Level 1/2 boundary) are indicated. Generally, this means that these are the specifications that could be violated if gains were lowered any further. Regarding the OLOP requirements, some cases have no open loop onset point which is indicated with a dash in the tables.

For all cases, the limiting specification in roll/pitch is the pitch crossover frequency, with the roll bandwidth also on the Level 1/2 boundary. For the aircraft held to the standard specifications, the command model following is limiting for both roll and pitch, but when held to the Froude-scaled requirements, the disturbance rejection bandwidth is limiting instead. Based on the actuator RMS values in roll/pitch, it can be seen that the aircraft held to the scaled specifications require more actuator effort than the unscaled cases at the same size. This is a result of the changes in boundaries for the scaled requirements.

In yaw, the limiting metrics are bandwidth and crossover frequency for all aircraft cases. For piloted input, the values of the actuator RMS are lower for the unscaled aircraft. As the requirements are scaled for the smaller vehicles, their actuator activity increases (as measured by actuator RMS). The yaw actuator RMS is substantially larger for all configurations than pitch, suggesting a relative lack of authority in this axis.

The current margins required to meet the Level 1 OLOP specifications are given in Table 8. Though there is no onset point for the nominal installed current margin ($\Delta i/i_{\text{hover}} = 1$), the limiting OLOP specification for the inner loop is the pilot yaw input for all cases except the largest aircraft which is limited by the roll disturbance OLOP requirement.

Table 6: Inner Loop Handling Qualities (Roll/Pitch)

Parameter	Units	1.2 m	1.2 m Scaled	1.8 m	1.8 m Scaled	2.4 m
Stability Gain Margin	dB	11	13	12	12	13
Stability Phase Margin	deg	51	57	53	57	49
Bandwidth	rad/s	2.5*	3.5*	2.5*	2.9*	2.5*
Phase Delay	s	0.067	0.044	0.070	0.057	0.084
Crossover Frequency	rad/s	5.0†	7.1†	5.0†	5.8†	5.0†
Disturbance Rejection Bandwidth	rad/s	1.2	1.3*	1.1	1.1*	1.2
Disturbance Rejection Peak	dB	3.5	3.5	3.3	3.5	3.3
Command Model Following	—	49*†	42	49*†	34	49*†
OLOP Phase (Pilot)	dB	-	-	-	-	-
OLOP Magnitude (Pilot)	deg	-	-	-	-	-
OLOP Phase (Disturbance)	dB	-	-144	-	-153	-137
OLOP Magnitude (Disturbance)	deg	-	-11.4	-	-15.0	-4.4
Actuator RMS (Pilot)	—	0.029	0.082	0.044	0.073	0.049
Actuator RMS (Disturbance)	—	0.053	0.111	0.074	0.098	0.113

* Limiting in roll † Limiting in pitch - No open loop onset point in frequency range

Table 7: Inner Loop Handling Qualities (Yaw)

Parameter	Units	1.2 m	1.2 m Scaled	1.8 m	1.8 m Scaled	2.4 m
Stability Gain Margin	dB	37	32	35	34	36
Stability Phase Margin	deg	90	101	102	106	109
Bandwidth	rad/s	1.4*	2.0*	1.4*	1.6*	1.4*
Phase Delay	s	0.002	0.002	0.002	0.002	0.002
Crossover Frequency	rad/s	5.0*	7.1*	5.0*	5.8*	5.0*
Disturbance Rejection Bandwidth	rad/s	1.0	1.4	1.0	1.1	1.0
Disturbance Rejection Peak	dB	0.19	0.19	0.23	0.25	0.27
Command Model Following	—	0.08	0.23	0.07	0.08	0.07
OLOP Phase (Pilot)	dB	-	-	-	-	-
OLOP Magnitude (Pilot)	deg	-	-	-	-	-
OLOP Phase (Disturbance)	dB	-79	-82	-67	-71	-65
OLOP Magnitude (Disturbance)	deg	-6.01	-1.04	-3.45	-1.02	-2.27
Actuator RMS (Pilot)	—	0.080	0.161	0.087	0.114	0.095
Actuator RMS (Disturbance)	—	0.49	1.16	0.47	0.67	0.45

* Limiting in yaw

- No open loop onset point in frequency range

Table 8: Inner Loop OLOP Current Requirements

Rotor Diameter (m)	Required Current ($\Delta i/i_{\text{hover}}$)	Limiting Input
1.2	0.27	Pilot Yaw
1.2 (Scaled)	0.57	Pilot Yaw
1.8	0.34	Pilot Yaw
1.8 (Scaled)	0.45	Pilot Yaw
2.4	0.51	Roll Disturbance

Inner Loop Time Domain Simulations (ACAH/RCDH)

Two simulations are considered along the roll/pitch axes in hover: a doublet input in pitch attitude and a gust. The longitudinal and lateral dynamics are identical but for a 18% higher inertia in pitch (Table 2). Thus, only pitch and yaw results are presented for the inner loop controller in hover.

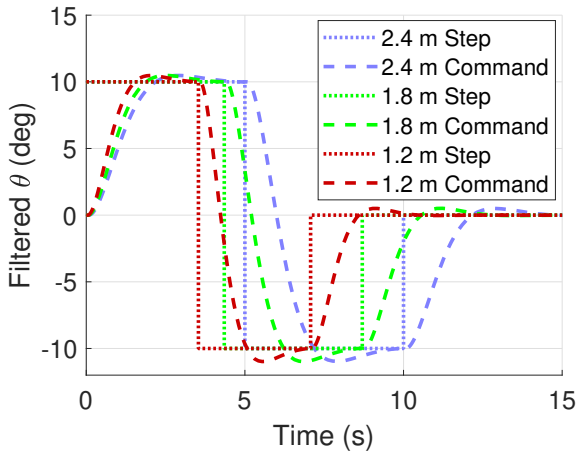

Figure 4: Filtered Pitch Attitude Doublet Input

Pitch Doublet: Figure 4 shows a 10° doublet input (before and after the second-order command filter) in the commanded pitch attitude of the quadcopters. The dotted lines indicate the unfiltered step command, while the dashed lines show the filtered command. The magnitude of the doublet does not scale with the size of the quadcopter, but the doublet's duration and the frequency of the command models do. Thus, the smaller quadcopters follow the step more aggressively. For the comparison of the quadcopters without scaling the HQ requirements, the input given to the largest quadcopter is given to all vehicles.

The closed-loop vehicle responses to the doublet input are plotted in Fig. 5. When all quadcopters are tuned to the same requirements, they all follow the same trajectory (Fig. 5a), settling to their steady-state value in roughly 4 seconds. When the HQ metrics are Froude-scaled, the smaller quadcopters respond more quickly, though they settle to the same attitude (Fig. 5b).

The current required by the rear-left rotor (Motor 3 in Fig. 1) during the pitch doublet is plotted in Fig. 6, normalized by hover current. Each step change in the doublet (at $t = 0$, $t = 5s$, and $t = 10s$ for the 2.4 m quadcopter) is accompanied by a spike in the current required, as the system tries to rapidly change the rotor thrust through change in rotor speed.

When Froude-scaling is applied to the HQ requirements for the smallest aircraft, the magnitude of this spike is around 0.5 for a 20 degree change in the commanded pitch attitude (0.025 per degree), but around 0.3 for the largest aircraft (0.015 per degree). This results from the more aggressive command models on the smaller aircraft. Conversely, when all vehicles are held to the same HQ requirements, the smallest vehicle requires the least current margin. Motor power (not pictured) follows a similar trend. The maximum values of both the normalized current and power are reported for each configuration in Table 9.

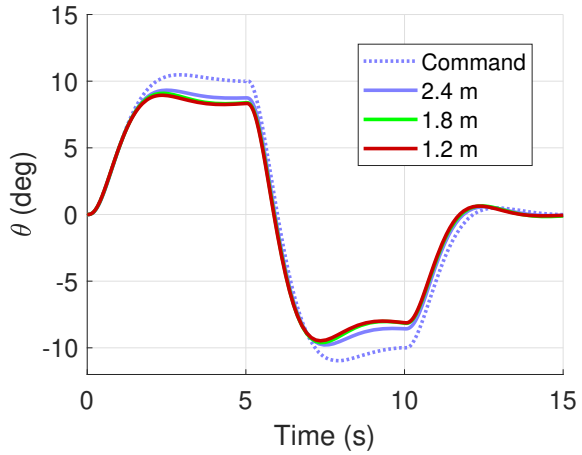

(a) Aircraft Held to Manned-Sized HQ Requirements

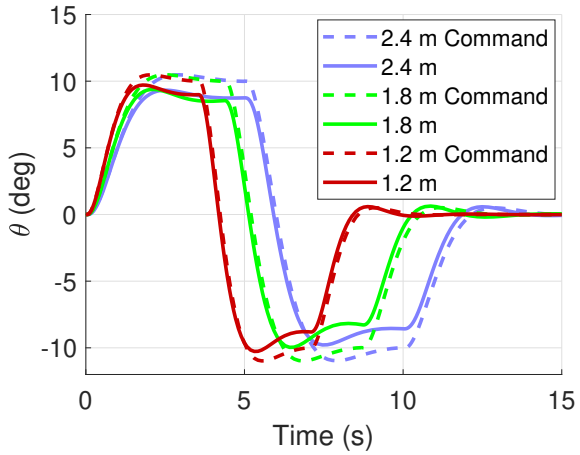

(b) Aircraft Held to Scaled HQ Requirements

Figure 5: Pitch Attitude Response to Doublet Input

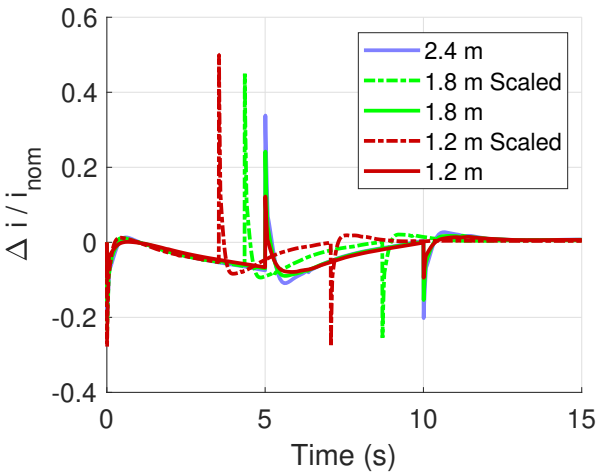

Figure 6: Motor 3 Current for Pitch Doublet

Table 9: Maximum Motor Input During Pitch Doublet

Rotor Diameter (m)	Max $\Delta i/i_{\text{nom}}$	Max $\Delta P/P_{\text{nom}}$
1.2	0.12	0.16
1.2 (Scaled)	0.50	0.59
1.8	0.24	0.29
1.8 (Scaled)	0.45	0.52
2.4	0.33	0.39

Inner Loop Longitudinal Gust: A longitudinal gust is applied to the aircraft in hover to examine how the inner loop controller responds to a disturbance in pitch attitude. The gusts take a 1-cosine shape (Ref. 13), with the frequency chosen to maximize motor effort. This is done by examining the frequency response of input gust to actuator effort (Fig. 7) and choosing the frequency that results in the highest magnitude. This will represent a reasonable worst-case scenario for motor sizing.

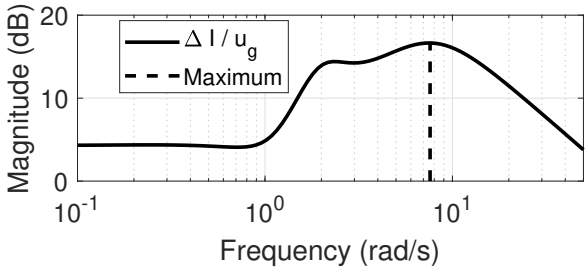

Figure 7: Magnitude Frequency Response from Longitudinal Gust to Motor Current

These worst-case gusts for each aircraft case have the parameters given in Table 10 and are shown in Fig. 8. When the HQ metrics are scaled, so too is the magnitude of the gust (larger aircraft are expected to reject larger gusts). Gusts are represented along the aircraft body-reference axis. Thus, a positive longitudinal gust is a tailwind.

Table 10: Longitudinal Gust Parameters (Attitude Hold)

Rotor Diameter (m)	Frequency (rad/s)	Duration (s)
1.2	6.4	0.98
1.2 (Scaled)	10.4	0.60
1.8	6.7	0.94
1.8 (Scaled)	8.5	0.74
2.4	6.6	0.95

The vehicle pitch attitude during the gust is plotted in Fig. 9. The initial response of the vehicles is to pitch nose down, and then nose up as the attitude-hold controller brings the pitch attitude back to zero.

The current input to the front-right motor (Motor 1 in Fig. 1) during the gust is plotted in Fig. 10. The input to the front motors is increased (and the rear decreased) to create a restorative moment that brings the pitch attitude back to zero, with some

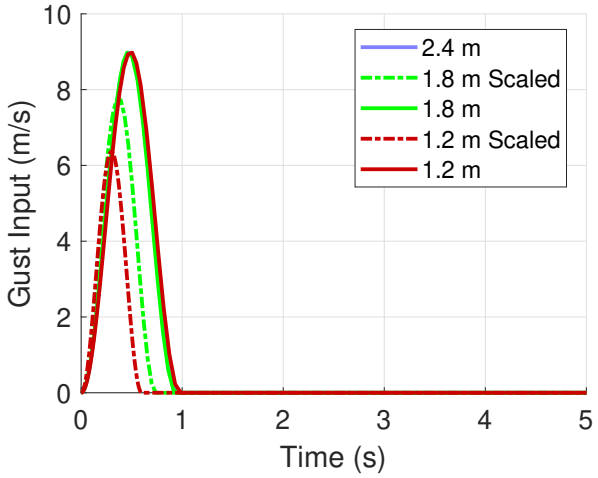

Figure 8: Longitudinal Gust Input (Attitude Hold)

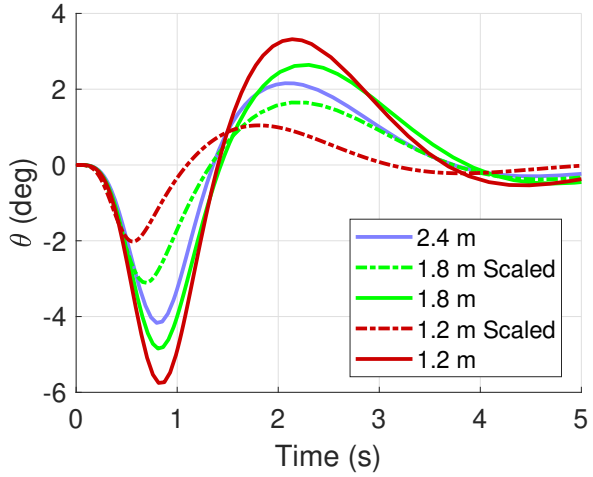

Figure 9: Pitch Attitude Response (Longitudinal Gust)

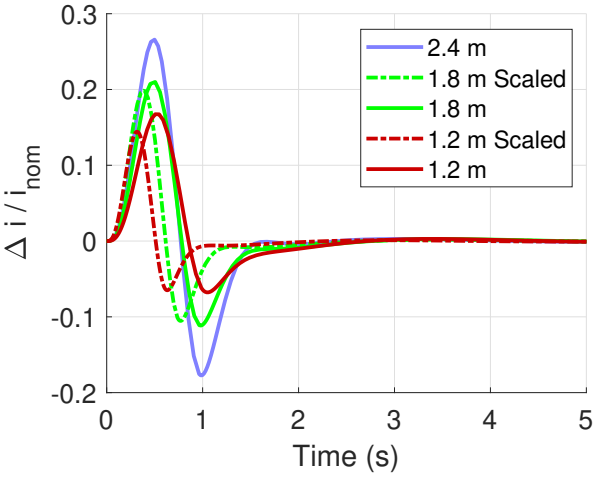

Figure 10: Motor 1 Current for Longitudinal Gust (ACAH)

overshoot as the gust subsides. For the unscaled cases, the magnitude of this input is higher for the larger aircraft as they need to overcome greater rotor inertia. For the scaled aircraft, the smaller magnitude gust requires less corrective input than the unscaled cases of the same size. This suggests that with Froude-scaling, larger quadcopters will require more margin to reject gust disturbances.

The maximum values of the current and power margin required to reject the gust are given in Table 11. Compared to the current required to execute the doublet maneuver, relatively little current and power input is needed for all aircraft to respond to the longitudinal gust; no vehicle requires more than 27% of the hover current during the longitudinal gust presented (3% per m/s of gust magnitude). This suggests that rejection of such gusts will not be an issue unless significantly larger gust magnitudes are considered.

Table 11: Maximum Current and Power Input to Motor 1 During Longitudinal Gust (ACAH)

Rotor Diameter (m)	Max $\Delta i/i_{\text{nom}}$	Max $\Delta P/P_{\text{nom}}$
1.2	0.17	0.29
1.2 (Scaled)	0.14	0.24
1.8	0.21	0.33
1.8 (Scaled)	0.20	0.31
2.4	0.27	0.40

Yaw Rate Step: Truncated step commands in yaw rate are simulated. Figures 11 and 12 show the yaw rate and heading response, respectively. All aircraft are able to follow the filtered yaw rate and heading command precisely. The magnitude of the step is determined via Froude-scaling (smaller vehicles are expected to change heading more quickly), and the length of the step is set such that the commanded heading change is 100°. Additionally, the time constant of the first-order command filter is lower for the smaller vehicles than for the larger ones (due to higher bandwidth requirements).

The change in current input to the front-right motor during the truncated yaw rate step is shown in Fig. 13 for each aircraft configuration. An initial spike in current is seen around $t = 0$ s as the vehicles increase the torque to the counterclockwise motors (and decrease torque to the clockwise motors) to produce a net moment that rotates the aircraft and achieves the desired yaw rate. A second, negative peak is seen when the step input is truncated. The negative input produces a net torque in the opposite direction, slowing the aircraft until it has stopped rotating.

The peak values of current and power required for the 5 aircraft cases to track a truncated step in yaw rate are summarized in Table 12. For the aircraft held to the same HQ specifications and given the same step input, the larger aircraft require more current margin due to their higher vehicle inertia.

When held to the scaled HQ specifications and given scaled step inputs, the smaller aircraft require a significantly (twice as much, for the smallest quadcopter) larger change in input

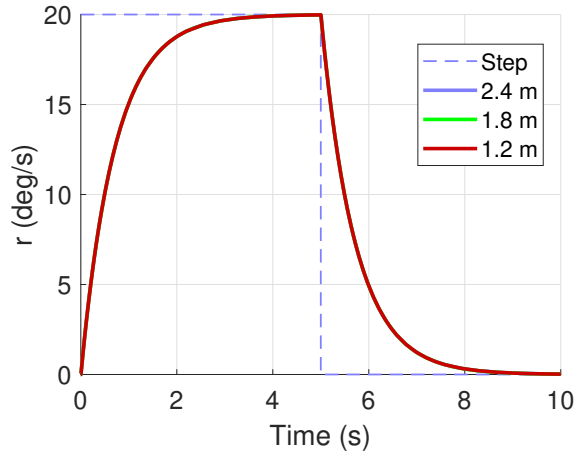

(a) Aircraft Held to Manned-Sized HQ Requirements

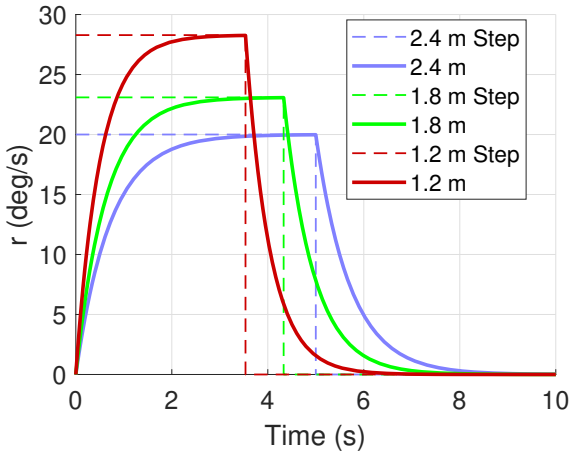

(b) Aircraft Held to Scaled HQ Requirements

Figure 11: Yaw Rate Response to Truncated Step Input

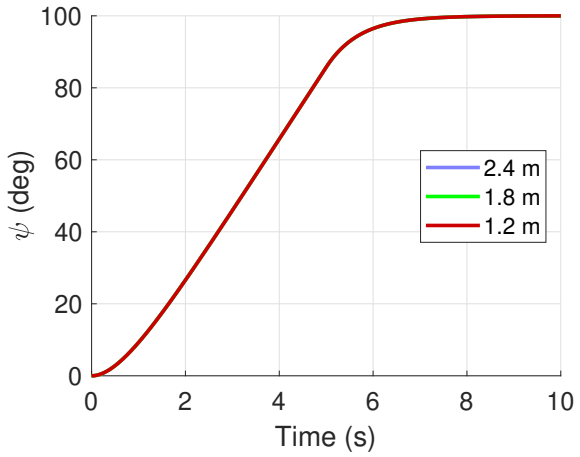

(a) Aircraft Held to Manned-Sized HQ Requirements

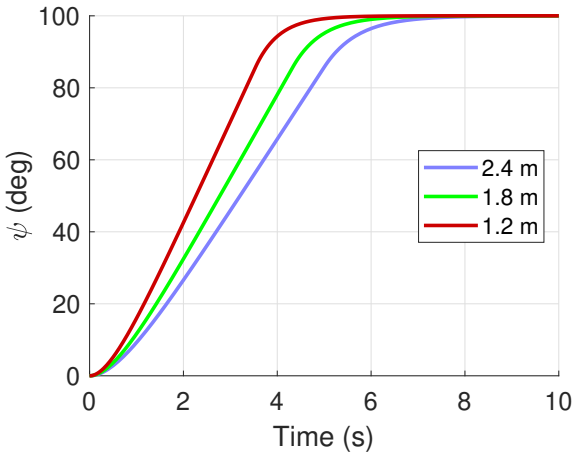

(b) Aircraft Held to Scaled HQ Requirements

Figure 12: Heading Response to Truncated Step Input

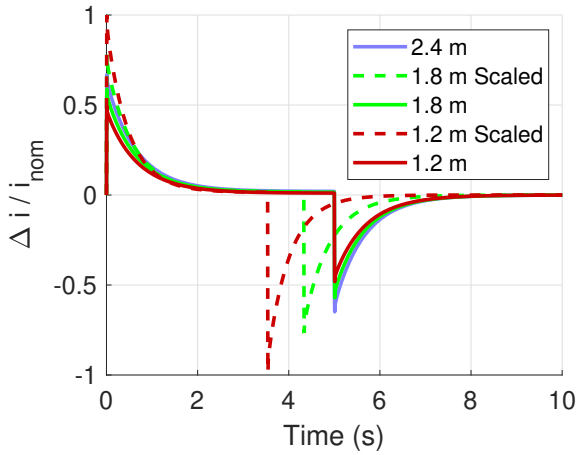

Figure 13: Motor 1 Current for Truncated Yaw Rate Step

Table 12: Maximum Current and Power Input to Motor 1 During Truncated Yaw Rate Step

Rotor Diameter (m)	Max $\Delta i/i_{\text{nom}}$	Max $\Delta P/P_{\text{nom}}$
1.2	0.49	0.62
1.2 (Scaled)	1.00	1.23
1.8	0.59	0.72
1.8 (Scaled)	0.78	0.96
2.4	0.67	0.82

current relative to the hover value. This is a result of a of higher expectations in both yaw rate (smaller aircraft are given larger yaw rate commands) and bandwidth (smaller vehicles are expected to react to commanded yaw rates more quickly). This suggests a lack of yaw authority from the smaller rotors, as the smaller motors struggle to produce enough change in torque to turn the aircraft.

Outer Loop Control Design

As described in Ref 11, after the ACAH controller is tuned, the inner loop gains are frozen, and an outer loop Transnational Rate Command (TRC) controller is added to the longitudinal/lateral and vertical axes of the aircraft. The specifications used to optimize the TRC controller are listed in Table 4.

Tables 13 and 14 give the optimized values of the HQ specifications along the longitudinal/lateral and vertical axes respectively. Since the aircraft are nearly identical along the longitudinal and lateral axes in hover, the same command models and controller gains are used for both axes.

For the longitudinal and lateral axes, the command model is designed such that the value of the rise time falls on the Level 1/2 boundary. The crossover frequency and disturbance rejection peak are the limiting specification, regardless of whether Froude-scaling is applied to the specifications. In heave, the command model is designed so that the heave mode pole falls on the Level 1/2 boundary. The crossover frequency and disturbance rejection bandwidth are limiting in heave.

As was seen with the inner loop, the outer loop actuator RMS metrics indicate that aircraft held to scaled HQ requirements require more actuator effort than those held to unscaled requirements.

Table 15: Outer Loop OLOP Current Requirements

Rotor Diameter (m)	Required Current ($\Delta i / i_{\text{hover}}$)	Limiting Input
1.2	0.05	Heave Disturbance
1.2 (Scaled)	0.10	Heave Disturbance
1.8	0.08	Heave Disturbance
1.8 (Scaled)	0.12	Heave Disturbance
2.4	0.10	Heave Disturbance

Table 13: Outer Loop Handling Qualities (Longitudinal/Lateral)

Parameter	Units	1.2 m	1.2 Scaled	1.8 m	1.8 m Scaled	2.4 m
Stability Gain Margin	dB	8.9	8.5	8.4	8.9	8.4
Stability Phase Margin	deg	62	56	60	60	55
Crossover Frequency	rad/s	1.0*†	1.4*†	1.0*†	1.2*†	1.0*†
Disturbance Rejection Bandwidth	rad/s	0.63	0.85	0.61	0.69	0.60
Disturbance Rejection Peak	dB	5.0*†	5.0*†	5.0*†	5.0*†	5.0*†
Rise Time	s	5.0*†	3.4*†	5.0*†	4.2*†	5.0*†
Command Model Following	-	9.1	3.5	9.5	7.1	6.1
OLOP Phase (Pilot)	deg	-	-327	-332	-309	-284
OLOP Magnitude (Pilot)	dB	-	-75	-81	-46	-33
OLOP Phase (Disturbance)	deg	-189	-160	-168	-155	-159
OLOP Magnitude (Disturbance)	dB	-10	-5.7	-6.7	-5.2	-5.5
Actuator RMS (Pilot)	-	0.07	0.11	0.11	0.14	0.15
Actuator RMS (Disturbance)	-	0.34	0.57	0.47	0.69	0.62

* Limiting in longitudinal axis † Limiting in lateral axis

Table 14: Outer Loop Handling Qualities (Heave)

Parameter	Units	1.2 m	1.2 m Scaled	1.8 m	1.8 m Scaled	2.4 m
Stability Gain Margin	dB	51	47	51	49	51
Stability Phase Margin	deg	88	82	86	84	87
Crossover Frequency	rad/s	1.0*	1.6	1.0*	1.2*	1.0*
Disturbance Rejection Bandwidth	rad/s	1.0*	1.4*	1.0*	1.2*	1.0*
Disturbance Rejection Peak	dB	0.63	0.83	0.63	0.73	0.63
Heave Mode Pole	rad/s	0.20*	0.29*	0.20*	0.23*	0.20*
Time Delay	s	0.089	0.085	0.089	0.088	0.089
Command Model Following	-	0.012	0.006	0.012	0.009	0.012
OLOP Phase (Pilot)	deg	-	-	-	-	-
OLOP Magnitude (Pilot)	dB	-	-	-	-	-
OLOP Phase (Disturbance)	deg	-107	-106	-102	-102	-99
OLOP Magnitude (Disturbance)	dB	-10.2	-6.3	-6.8	-5.0	-4.7
Actuator RMS (Pilot)	-	0.05	0.06	0.07	0.08	0.10
Actuator RMS (Disturbance)	-	0.47	0.52	0.65	0.70	0.84

* Limiting in heave - No open loop onset point in frequency range

The minimum current margin required to meet the Level 1 OLOP requirements are given in Table 15. For all cases, the heave disturbance onset point is the first to reach the Level 1/2 boundary. Significantly less current margin is required to meet the outer loop OLOP requirements than the inner loop OLOP requirements (Table 8).

Outer Loop Time Domain Simulations (TRC)

Similar to the inner loop, two time domain simulations are considered in along the longitudinal/lateral axes, with only the longitudinal results presented. A small magnitude step (nominally 5 m/s, 9.7 kt) in longitudinal flight speed is simulated, as well as a longitudinal gust. The outer loop also controls the heave rate of the aircraft, so a step change in heave rate (nominally 5 m/s, 984 ft/min) and a vertical gust are also simulated.

Longitudinal Velocity Step: The aircraft response to a step command in longitudinal velocity is plotted in Fig. 14 for all cases. Command model following for all vehicles is excellent (Table 13), so the filtered commands are omitted. The aircraft that are all held to the manned-sized HQ requirements follow the same step change in flight speed while the aircraft held to Froude-scaled requirements follow a scaled step. With the application of Froude-scaling, the smaller aircraft are not required to go as fast as the larger aircraft, though they are required to settle more quickly (as a result of the scaled rise time specification).

In order to achieve the desired longitudinal flight speed, the quadcopters increase the input to the rear rotors and decrease the input to the front rotors. This pitches the aircraft nose-down, tilting the rotor plane and accelerating the aircraft forward. This pitch response is shown in Fig. 15, with the maximum pitch attitude for all aircraft cases being between -8 and -10 degrees during the step.

The normalized change in current input to the rear-left rotor during the step in longitudinal velocity is plotted in Fig. 16. The input current peaks quickly during the aircraft responses as the controller attempts to pitch the aircraft and accelerate forward. The maximum values of required current and power margin (which follows a similar trend as the current) are given in Table 16.

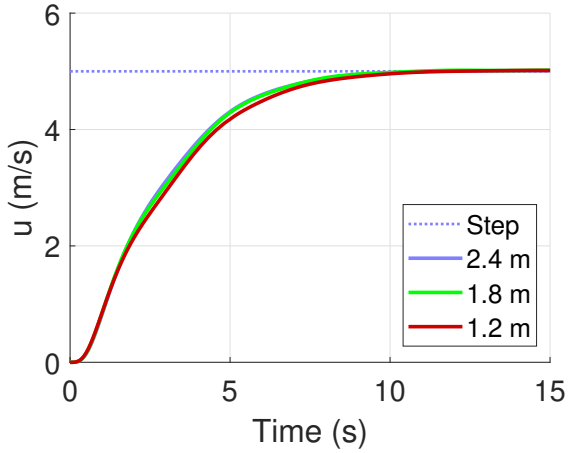

(a) Aircraft Held to Manned-Sized HQ Requirements

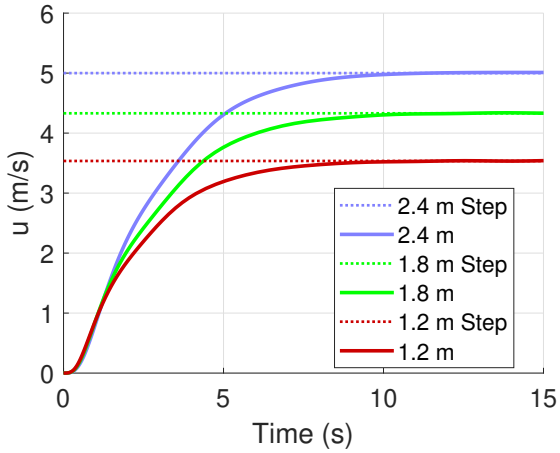

(b) Aircraft Held to Scaled HQ Requirements

Figure 14: Longitudinal Velocity Step Response

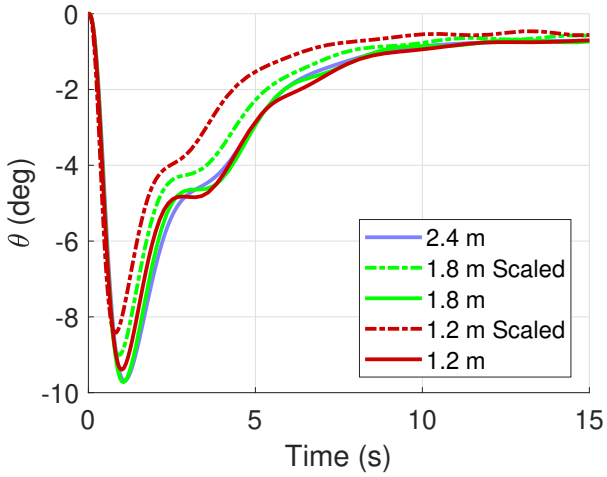

Figure 15: Pitch Attitude During Longitudinal Velocity Step

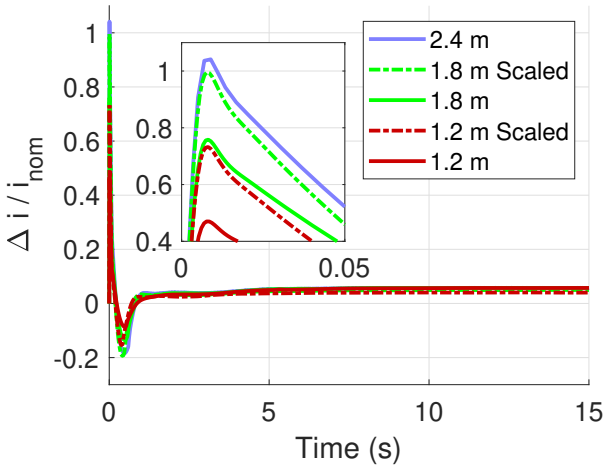

Figure 16: Motor 3 Current for Longitudinal Velocity Step

Table 16: Maximum Current and Power Input to Motor 3 During Longitudinal Step

Rotor Diameter (m)	Max $\Delta i/i_{\text{nom}}$	Max $\Delta P/P_{\text{nom}}$
1.2	0.47	0.59
1.2 (Scaled)	0.73	0.90
1.8	0.76	0.93
1.8 (Scaled)	1.00	1.22
2.4	1.04	1.27

Even with this relatively small magnitude step, the 544 kg aircraft and 308 kg aircraft held to the scaled specifications require a change in current input greater than the nominal hover value ($\Delta i/i_{\text{hover}} > 1$). Though the maximum magnitude of the pitch attitude is similar to the inner loop commands, the frequency of the inner loop command model must be greater in TRC mode than in ACAH mode, due to phase margin requirements on the outer loop. Thus, the vehicle responds to the commanded pitch attitude more aggressively, requiring greater current than was seen in the pitch doublet command.

Outer Loop Longitudinal Gust: Similar to what was done with the ACAH controller, a longitudinal gust disturbance is simulated in order to examine the aircraft response. The gust frequencies are chosen based on the magnitude frequency response of the input gust frequency to motor current (similar to Fig. 7). These worst-case gust parameters are given in Table 17.

Table 17: Longitudinal Gust Parameters for Peak Magnitude Current Input (TRC)

Rotor Diameter (m)	Frequency (rad/s)	Duration (s)
1.2	6.4	0.98
1.2 (Scaled)	8.0	0.79
1.8	6.6	0.95
1.8 (Scaled)	7.4	0.85
2.4	6.7	0.94

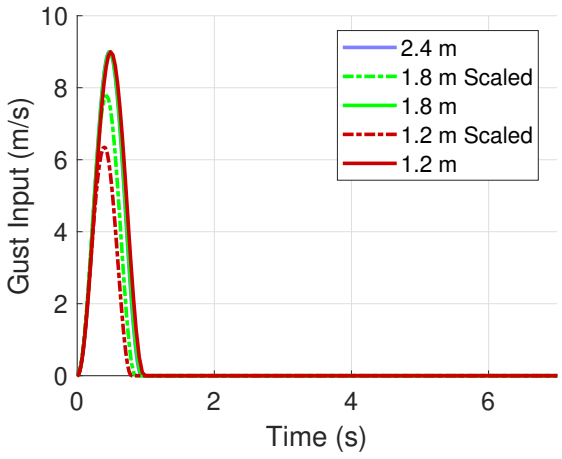

Figure 17: Longitudinal Gust Input (TRC)

The gust inputs for each aircraft case is shown in Fig. 17. The unscaled cases receive the same gust magnitude, while the cases held to the scaled HQ requirements receive gusts with Froude-scaled magnitude.

The vehicle pitch attitude during the gust is plotted in Fig. 18 and the longitudinal velocity is plotted in Fig. 19. The gust causes the aircraft to pitch nose-down and begin moving forward. The controllers attempt to return the aircraft to a stationary hover by pitching nose-up to slow the aircraft. With some oscillation, all aircraft cases are brought back to hover in roughly 8 seconds, with the small vehicles settling faster when their HQ specifications are Froude-scaled.

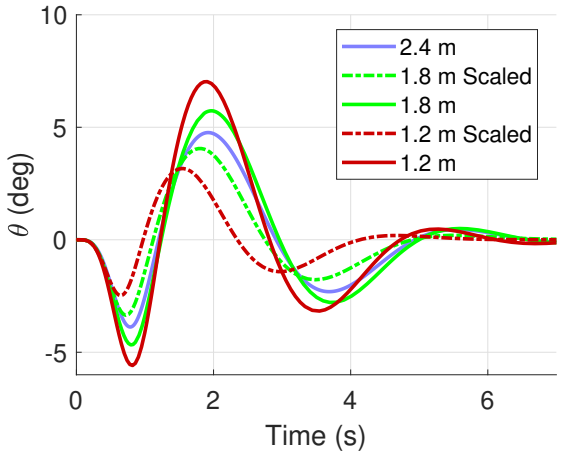

Figure 18: Pitch Response to Longitudinal Gust (TRC)

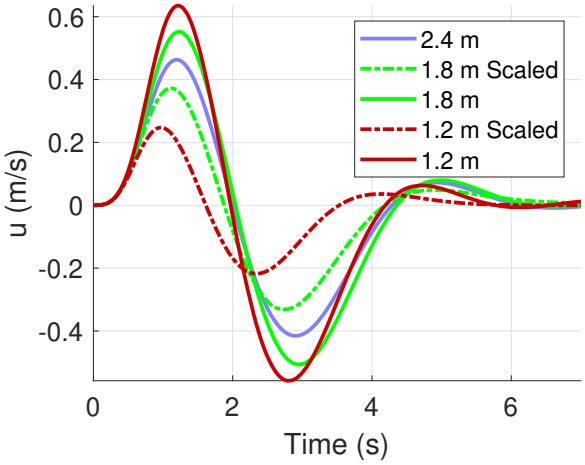

Figure 19: Response to Longitudinal Gust (TRC)

Figure 20 shows the normalized change in current input to the front-right rotor for each vehicle case during the longitudinal gust with a TRC controller. Similar to the inner loop longitudinal gust (with ACAH), the required changes in current for the aircraft to reject the gust are relatively small. The power input (not pictured) follows a similar trend to the current, and the required values of the current and power margin to reject the longitudinal gust are given in Table 18. The values of

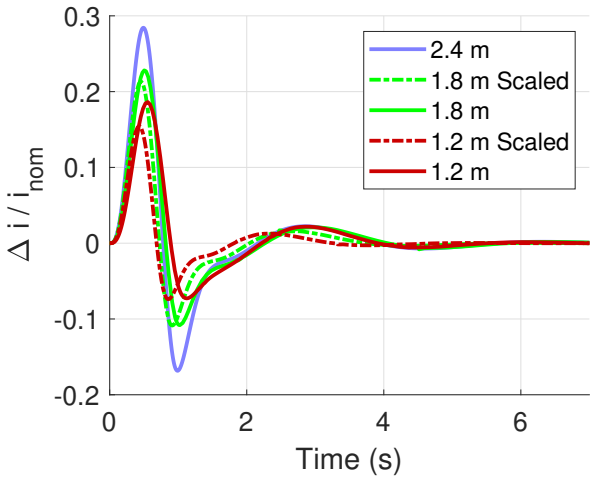

Figure 20: Current to Motor 1 for Longitudinal Gust (TRC)

Table 18: Maximum Current and Power Input to Motor 1 During Longitudinal Gust (TRC)

Rotor Diameter (m)	Max $\Delta i/i_{\text{nom}}$	Max $\Delta P/P_{\text{nom}}$
1.2	0.19	0.32
1.2 (Scaled)	0.15	0.26
1.8	0.23	0.36
1.8 (Scaled)	0.21	0.33
2.4	0.28	0.42

the required current and power margin for the TRC controller are approximately the same (within 2% I_{nom}) as those for the attitude-hold controller.

Heave Step: A step change in climb rate is simulated on each aircraft case. The step command is filtered to meet the heave response time constant specification. The aircraft are able to accurately follow the filtered command (Fig. 21). The unscaled cases all have the same response, achieving the desired climb rate of 5 m/s (984 ft/min) in about 20 s. For the aircraft held to the Froude-scaled specifications, the smaller aircraft are required to reach a lower velocity in a smaller amount of time.

The normalized changes in current input to a single motor during the heave step are shown in Fig. 22. For all cases, the input current to all motors spikes at the beginning of the step as the controller attempts to increase the thrust produced by all rotors to accelerate the aircraft upward, and then settles as the aircraft reach the desired heave rate. The maximum values of both current and power margin required given in Table 19.

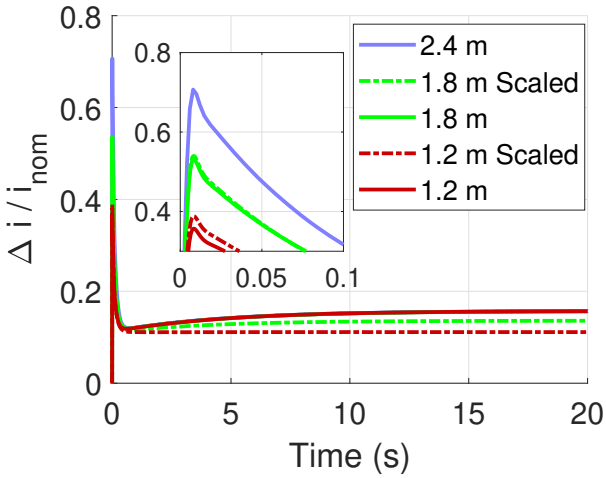

Figure 22: Current Input to Motor 1 During Heave Step

As was the case in the longitudinal axis, the larger aircraft require a larger change in input current, as the larger rotational inertia necessitates greater input to speed up the larger rotors and produce the required change in thrust.

The Froude-scaled cases require marginally more input than the unscaled cases with the same vehicle size, again due to the

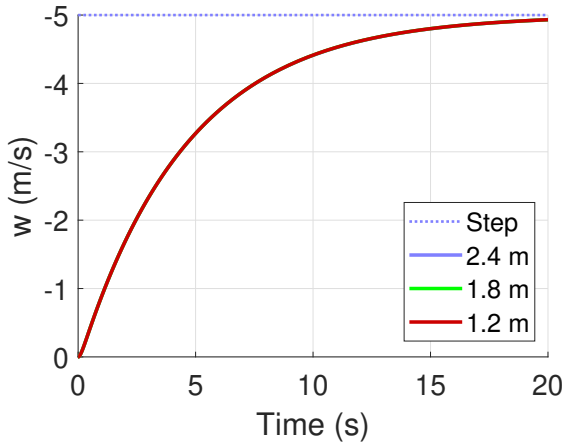

(a) Aircraft Held to Manned-Sized HQ Requirements

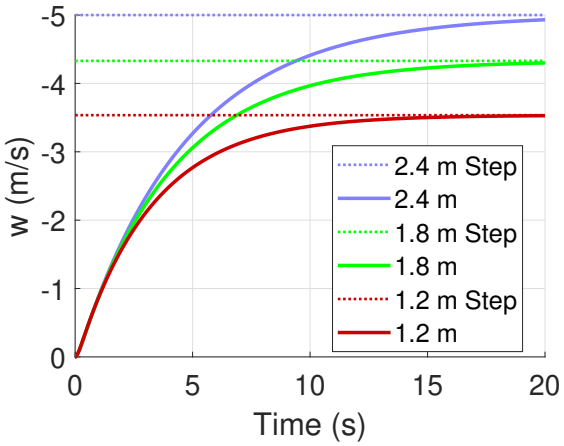

(b) Aircraft Held to Scaled HQ Requirements

Figure 21: Climb Rate Step Response

Table 19: Maximum Current and Power Input to Motor 1 During Heave Step

Rotor Diameter (m)	Max $\Delta i/i_{\text{nom}}$	Max $\Delta P/P_{\text{nom}}$
1.2	0.36	0.46
1.2 (Scaled)	0.39	0.49
1.8	0.53	0.66
1.8 (Scaled)	0.54	0.67
2.4	0.71	0.86

more aggressive time constant and time delay that the Froude-scaled metrics require. The scaled cases must accelerate faster in order to fit the desired response. The smaller aircraft still require less current margin than the larger, even with more aggressive controllers.

Though the heave step does not limit the individual rotor current capability, it is important to consider that in heave this change in current is required to all rotors, whereas in every other axis the current increase to two motors is offset by an equal decrease in the two others. This means that the heave axis will set battery current requirements.

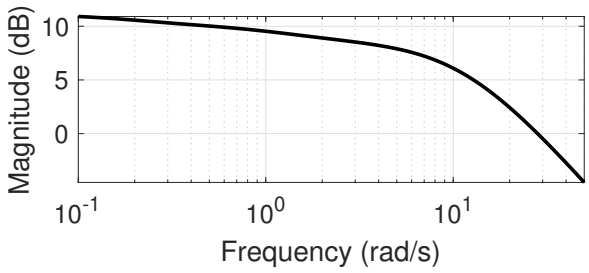

Figure 23: Bode Plot of Input Vertical Gust to Motor 1 Current

Vertical Gust: Unlike the longitudinal gusts presented previously, the magnitude frequency for input vertical gust to actuator effort has no clear peak (Fig. 23). The magnitude increase with lower frequency gusts, meaning that a sustained wind will require the most actuator effort, rather than a short-term gust. Since there is no peak, a step change in gust magnitude is used. The Froude-scaled cases still receive gusts with scaled magnitude, shown in Fig. 24.

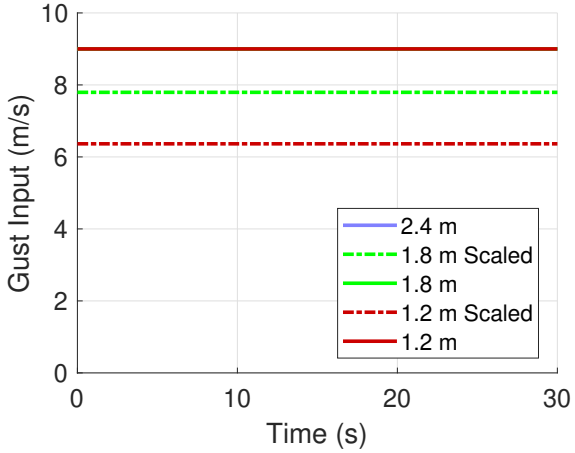

Figure 24: Vertical Gust Input

Figure 25 shows the aircraft responses to the vertical wind and Fig. 26 shows the normalized change in current input to a single motor. The positive gust magnitude is a downdraft on the aircraft, which cases the rotors to lose thrust. As the aircraft starts to descend (positive w), the controller increases the collective input to the motors in order to produce more thrust and brings the heave rate back to zero.

All three aircraft sizes held to the same handling qualities specifications have the same heave response and normalized current input when given the vertical wind. The aircraft held to the scaled HQ specifications are given a lower magnitude wind and have a lower magnitude response and normalized current input.

The required values of current and power margin for each aircraft case to reject the heave gust are given in Table 20. When

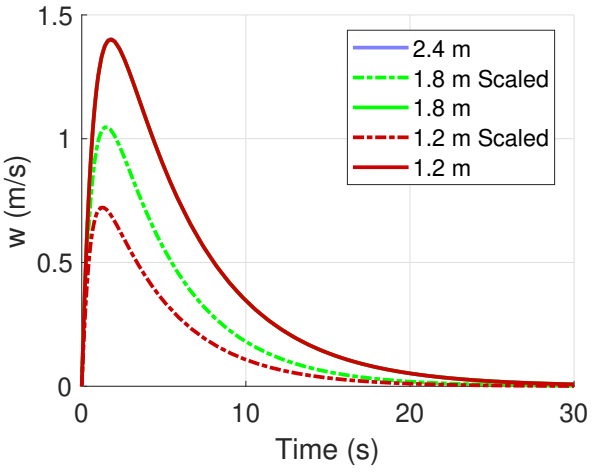

Figure 25: Response to Vertical Gust

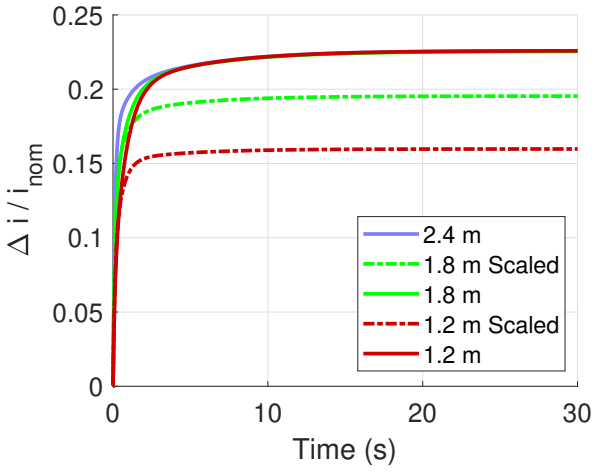

Figure 26: Current Input to Motor 1 During Vertical Gust

given the same magnitude gust, all vehicles require the same current margin over hover, and the current requirement scales linearly with the gust magnitude.

Table 20: Maximum Current and Power Input to Motor 1 During Vertical Wind

Rotor Diameter (m)	Max $\Delta i/i_{\text{nom}}$	Max $\Delta P/P_{\text{nom}}$
1.2	0.23	0.44
1.2 (Scaled)	0.16	0.32
1.8	0.23	0.44
1.8 (Scaled)	0.20	0.38
2.4	0.23	0.44

Limiting Cases and Motor Weight

Required motor weight can be estimated from the maximum current requirement across all time domain simulations for each aircraft case. The required motor torque input is found by multiplying the maximum current (including hover current) by the torque constant. Motor weight can then be estimated using Eq. 10 (Ref. 14).

$$W_{eng} = 0.5382Q^{0.8129} \tag{10}$$

Based on Based on hover torque considerations only (from Table 2), the total weight of the motors would be 9.6 kg, 25.2 kg, and 51.2 kg for the smallest through largest quadcopter (corresponding to aircraft weight fractions of 7.1%, 8.2%, and 9.4%). This is calculated as a point of reference, to assess the weight increase associated with meeting handling qualities requirements.

Including both the hover and maneuvering torques, the time simulations that require the largest torque/current are summarized in Table 21, along with the estimated motor masses. Regardless of the scaling of the HQ specification, the smallest aircraft is limited by yaw rate commands, while the step change in longitudinal velocity requires the highest peak current input for the larger two aircraft. This difference is a result of the relative lack of yaw authority of the smaller rotors. The larger aircraft require a higher motor weight fraction than the smaller ones, with the largest quadcopter needing almost 17% of its gross weight to be motors, representing a 79% increase in motor weight fraction relative to motors sized for hover only. Naturally, the aircraft held to the Froude-scaled specifications require larger motors than the unscaled cases as a result of the stricter requirements, though the smaller aircraft still require an overall smaller weight fraction dedicated to motors.

If an ACAH controller is used in the longitudinal/lateral axes instead of the TRC controller for the larger two aircraft (the limiting case for the smallest will not change), the new limiting maneuvers are listed in Table 22. The aircraft with 1.8 m diameter motors requires the highest current input during the step in yaw rate, while the largest aircraft is limited by heave. Without TRC, the largest aircraft now requires about 15% motor weight fraction (a 54% increase relative to motors sized for hover only), and the smaller aircraft require less. As the smallest vehicle was not limited by the TRC controller, its required motor weight does not change.

CONCLUSIONS

Optimized inner and outer loop controllers were designed holding three quadcopters of different sizes to standard and Froude-scaled ADS-33 handling qualities specification. For the inner loop, all aircraft cases are able to meet the Level 1 HQ specifications along the roll/pitch axes with ACAH/RCDH control. In roll/pitch it was seen that:

Table 21: Maximum Current & Motor Mass with TRC

Rotor Diameter (m)	Maneuver	Maximum Current (A)	Maximum Torque (N-m)	Motor Mass Mass (kg, each)	Weight Fraction (%)	Weight Increase Over Hover Only (%)
1.2	Yaw Rate Step	112	34	3.3	9.7	37
1.2 (Scaled)	Yaw Rate Step	150	45	4.2	12.4	75
1.8	Longitudinal Velocity Step	197	130	10.0	13.0	59
1.8 (Scaled)	Longitudinal Velocity Step	224	148	11.1	14.4	76
2.4	Longitudinal Velocity Step	306	361	22.8	16.8	79

Table 22: Maximum Current & Motor Mass without TRC

Rotor Diameter (m)	Maneuver	Maximum Current (A)	Maximum Torque (N-m)	Motor Mass Mass (kg, each)	Weight Fraction (%)	Weight Increase Over Hover Only (%)
1.8	Yaw Rate Step	178	118	9.2	12.0	46
1.8 (Scaled)	Yaw Rate Step	199	132	10.1	13.1	60
2.4	Heave Rate Step	257	303	19.8	14.5	54

- The optimization of the roll/pitch controllers is limited by the roll bandwidth and pitch crossover frequency.
- When Froude scaling is applied, smaller aircraft require less current margin to reject a longitudinal gust than the larger aircraft, but the opposite is true for a doublet input in pitch attitude.

All cases are also able to meet the Level 1 HQ specifications with at RCDH controller in yaw. It was seen that:

- The optimization of the yaw controllers is limited by the yaw bandwidth and yaw crossover frequency.
- When Froude scaling is applied, the smaller aircraft require significantly higher current margin to follow a truncated step in yaw rate, suggesting a relative lack of yaw authority with the smaller rotors.

For the outer loop, all aircraft cases are able to meet the Level 1 HQ specifications with a TRC controller on the longitudinal/lateral axes. It was seen that:

- The optimization of the longitudinal/lateral TRC controller is limited by crossover frequency and disturbance rejection requirements.
- The larger aircraft, require large current margin during a small magnitude step command in longitudinal velocity as a result of the large rotational acceleration required, with the value of current margin exceeding 1 for the 2.4 m aircraft and Froude-scaled 1.8 m aircraft.
- Though higher than that of the ACAH control, rejection of a longitudinal/lateral gust with a TRC controller requires less current margin than following a step command in velocity.

All aircraft cases are also able to meet the Level 1 HQ specifications with a rate-command controller in heave. It was seen that:

- The optimization of the heave controller is limited by crossover frequency and disturbance rejection bandwidth.
- The larger aircraft require higher current margin during a step in heave rate than the smaller vehicles.
- The heave axis will be limiting for battery current requirements.
- The worst-case gust frequency in heave is a sustained wind, but even this requires relatively low current margin for all cases.

The values of maximum current input from the time simulations were used to estimate motor size. With TRC control, it was seen that the longitudinal velocity step was the maneuver that required the highest individual current input for the larger two aircraft cases as a result of the large pitch rotational acceleration required during the step, while the aircraft with 1.2 m rotors was limited by the yaw rate step. Using the maximum current values from this simulation, the aircraft with 1.2 m diameter rotors required 9.7% motor weight fraction (12.4% with scaled specifications), the aircraft with 1.8 m diameter rotors requires 13.0% motor weight fraction (14.4% with scaled specifications) and the aircraft with 2.4 m diameter rotors requires a motor weight fraction of 16.8%. Motor weight requirements can be somewhat reduced for the larger two aircraft by flying exclusively in ACAH mode instead of TRC mode. In this case, step commands in yaw rate are limiting for the 1.8 m aircraft (requiring 12.0% to 13.1% weight fraction) and heave commands are limiting for the largest vehicles, requiring 14.5% motor weight fraction.

ACKNOWLEDGMENTS

This work is carried out at Rensselaer Polytechnic Institute under the Army/Navy/NASA Vertical Lift Research Center of Excellence (VLRCOE) Program, grant number W911W61120012, with Dr. Mahendra Bhagwat as Technical Monitor. The authors would like to acknowledge the Army Combat Capabilities Development Command for sponsoring Ms. Walter through the Science Mathematics And Research Transformation Scholarship Program, as well as the Army Research Office for sponsoring Mr. McKay through the National Defense Science and Engineering Graduate Fellowship.

Author Contact:

Ariel Walter: waltea@rpi.edu
Michael McKay: mckaym2@rpi.edu
Robert Niemiec: niemir2@rpi.edu
Farhan Gandhi: fgandhi@rpi.edu
Christina Ivler: ivler@up.edu.

REFERENCES

1. Johnson, W., Silva, C., and Solis, E., "Concept Vehicles for VTOL Air Taxi Operations," AHS Technical Conference on Aeromechanics Design for Transformative Flight, San Francisco, CA, January 16–18, 2018.
2. "Aeronautical Design Standard, Performance Specification, Handling Qualities Requirements for Military Rotorcraft," Technical Report ADS-33E-PRF, March 2000.
3. Berger, T., Ivler, C., Berrios, M., Tischler, M., and Miller, D., "Disturbance Rejection Handling-Qualities Criteria for Rotorcraft," 72nd Annual AHS Forum, West Palm Beach, FL, May 16–19, 2016.
4. Walter, A., McKay, M., Niemiec, R., Gandhi, F., and Ivler, C., "Handling Qualities Based Assessment of Scalability for Variable-RPM Electric Multi-Rotor Aircraft," 75th Annual VFS Forum, Philadelphia, PA, May 13–16, 2019.

5. Ivler, C., Goerzen, C., Wagster, J., Sanders, F., Cheung, K., and Tischler, M., "Control Design for Tracking of Scaled MTE Trajectories on an IRIS+ Quadrotor," 74th Annual AHS Forum, Mesa, AZ, May 14–17, 2018.

6. Niemiec, R., and Gandhi, F., "Development and Validation of the Rensselaer Multicopter Analysis Code (RMAC): A Physics-Based Comprehensive Modeling Tool," 75th Annual VFS Forum, Philadelphia, PA, May 13–16, 2019.

7. Niemiec, R., *Development and Application of a Medium-Fidelity Analysis Code for Multicopter Aerodynamics and Flight Mechanics*, Ph.D. thesis, Rensselaer Polytechnic Institute, 2018.

8. Malpica, C., and Withrow-Maser, S., "Handling Qualities Analysis of Blade Pitch and Rotor Speed Controlled eVTOL Quadrotor Concepts for Urban Air Mobility," VFS International Powered Lift Conference 2020, San Jose, CA, January 21–23, 2020.

9. Niemiec, R., and Gandhi, F., "Multi-rotor Coordinate Transform for Orthogonal Primary and Redundant Control Modes for Regular Hexacopters and Octocopters," 42nd European Rotorcraft Forum, Lille, France, September 5–8, 2016.

10. Duda, H., "Flight Control System Design Considering Rate Saturation," *Aerospace Science and Technology*, Vol. 4, 1998, pp. 265–275.

11. Tischler, M., Berger, T., Ivler, C., Mansur, M., Cheung, K., and Soong, J., *Practical Methods for Aircraft and Rotorcraft Flight Control Design: An Optimization-Based Approach*, AIAA Education Series, Reston, VA, 2017.

12. Alvarenga, J., Vitzilaios, N., Rutherford, M., and Valavanis, K., "Scaled Control Performance Benchmarks and Maneuvers for Small-Scale Unmanned Helicopters," IEEE 54th Annual Conference on Decision and Control, Osaka, Japan, December 15–18, 2015.

13. Berrios, M., Berger, T., Tischler, M., Juhasz, O., and Sanders, F., "Hover Flight Control Design for UAS Using Performance-based Disturbance Rejection Requirements," AHS 73rd Annual Forum, Fort Worth, TX, May 9–11, 2017.

14. Johnson, W., "NDARC – NASA Design and Analysis of Rotorcraft," NASA TP 218751, April 2015.